




Article

Electrodeposited Copper Nanocatalysts for CO₂ Electroreduction: Effect of Electrodeposition Conditions on Catalysts' Morphology and Selectivity

Gianluca Zanellato *, Pier Giorgio Schiavi * , Robertino Zanoni, Antonio Rubino , Pietro Altimari and Francesca Pagnanelli 

Department of Chemistry, Sapienza University of Rome, Piazzale Aldo Moro n.5, 00185 Rome, Italy; robertino.zanoni@uniroma1.it (R.Z.); antonio.rubino@uniroma1.it (A.R.); pietro.altimari@uniroma1.it (P.A.); francesca.pagnanelli@uniroma1.it (F.P.)

* Correspondence: gianluca.zanellato@uniroma1.it (G.Z.); piergiorgio.schiavi@uniroma1.it (P.G.S.)

Abstract: Catalytic electroreduction of carbon dioxide represents a promising technology both to reduce CO₂ emissions and to store electrical energy from discontinuous sources. In this work, electrochemical deposition of copper on to a gas-diffusion support was tested as a scalable and versatile nanosynthesis technique for the production of catalytic electrodes for CO₂ electroreduction. The effect of deposition current density and additives (DAT, DTAB, PEG) on the catalysts' structure was evaluated. The selectivity of the synthesized catalysts towards the production of CO was evaluated by analyzing the gaseous products obtained using the catalysts as cathodes in electroreduction tests. Catalyst morphology was deeply influenced by the deposition additives. Copper nanospheres, hemispherical microaggregates of nanowires, and shapeless structures were electrodeposited in the presence of dodecyltrimethylammonium bromide (DTAB), 3,5-diamino-1,2,4-triazole (DAT) and polyethylene glycol (PEG), respectively. The effect of the deposition current density on catalyst morphology was also observed and it was found to be additive-specific. DTAB nanostructured electrodes showed the highest selectivity towards CO production, probably attributable to a higher specific surface area. EDX and XPS analysis disclosed the presence of residual DAT and DTAB uniformly distributed onto the catalysts structure. No significant effects of electrodeposition current density and Cu(I)/Cu(II) ratio on the selectivity towards CO were found. In particular, DTAB and DAT electrodes yielded comparable selectivity, although they were characterized by the highest and lowest Cu(I)/Cu(II) ratio, respectively.

Keywords: carbon dioxide electroreduction; copper electrodeposition; additive electrodeposition; morphology-controlled synthesis; copper nanocatalysts; gas diffusion electrode; carbon monoxide



Citation: Zanellato, G.; Schiavi, P.G.; Zononi, R.; Rubino, A.; Altimari, P.; Pagnanelli, F. Electrodeposited Copper Nanocatalysts for CO₂ Electroreduction: Effect of Electrodeposition Conditions on Catalysts' Morphology and Selectivity. *Energies* **2021**, *14*, 5012. <https://doi.org/10.3390/en14165012>

Academic Editor: Jesse Ko

Received: 30 April 2021

Accepted: 12 August 2021

Published: 15 August 2021

Publisher's Note: MDPI stays neutral with regard to jurisdictional claims in published maps and institutional affiliations.



Copyright: © 2021 by the authors. Licensee MDPI, Basel, Switzerland. This article is an open access article distributed under the terms and conditions of the Creative Commons Attribution (CC BY) license (<https://creativecommons.org/licenses/by/4.0/>).

1. Introduction

The anthropic emission of carbon dioxide is considered an issue of fundamental importance. Nowadays, both in scientific research and generalist media the decarbonization of industrial processes is an extensively treated topic.

Carbon dioxide emissions of human origin in 2019 were reported to be close to 34,000 million tons. Energy production systems based on fossil fuels are the direct cause of a considerable amount of these emissions, considering that nearly 85% of global energetic production relies on carbon-based compounds (natural gas, oil, coal, or their derivatives) [1]. In order to control and modify this trend, renewable energy sources are being taken into account but, due their intermittent production regime, large-scale energy storage systems are required. In addition, their application as energy sources does not fulfill the global demand for organic bulk chemicals, whose origin is completely linked to petroleum, natural gas and coal.

The necessary transition of the energy production from fossil fuels to renewable sources could benefit an electrochemical accumulation system targeted to the conversion of surplus electrical power to chemical compounds of global interest, a role that the electrocatalytic reduction of carbon dioxide (ERCO₂) could achieve.

The electroreductive processing of carbon dioxide involves the electrochemical conversion of CO₂ to light carbon compounds, such as carbon monoxide, hydrocarbons, and alcohols [2].

A peculiar trait of this process is its versatility: different organic compounds may be produced modifying the working parameters of the reduction cell or the structure of the cell cathode, i.e., its catalyst [3]. In the ERCO₂, the catalyst chemical composition and nanomorphology may affect selectivity and yield [4].

Currently, carbon monoxide is the principal product obtainable from selective catalysts able to reach exploitable currents [5]. Catalysts composed of single nickel atoms dispersed on activated carbon black [6] expressed faradaic efficiencies of the conversion to CO close to 100% during a 24 h reduction test. Other products of commercial interest consist of formic acid (mostly produced as formate, according to the electrolytic cell pH), ethanol, methane, and ethylene [7]. Hydrocarbons are most commonly produced from copper-based catalyst [8].

A large-scale application of this process requires a deeper understanding of the correlations between catalysts morphology and its activity. This could be possible only by obtaining metallic nanostructures with a defined nanomorphology, as a result of a versatile and scalable nanosynthesis technique. Galvanic electrodeposition, already widely used as production processes of metallic films and nanoparticles on to conductive supports, possess these features [9]. Electrodeposition techniques were applied to the production of ERCO₂ electrodes, proving to be a suitable synthesis pathway for efficient, selective and stable catalysts such as Ag-alloyed Zn dendritic electrodes [10] or copper–tin alloys [11]. If the deposition is applied on gas-permeable supports, such as carbon paper, electrodeposition could provide a simple and tunable synthesis technique for a so-called gas diffusion electrode (GDE) [12]. GDEs are commonly used in gas-liquid electrochemical cells, and various applications (e.g., water splitting cells, fuel cells) already benefit of this technical solution [13]. Being GDEs designed for gas-liquid electrochemical reactions, their use was evaluated in the context of ERCO₂. A catalyst composed of carbon and copper nanoparticles applied on a PTFE-based gas diffusive layer proved to be an efficient catalyst for the production of ethylene [14]. Nickel based GDEs proved to be selective and efficient catalysts for the production of carbon monoxide [15] while ethylene and carbon monoxide were also produced using a GDE composed of copper sputtered on a carbon-based support [16].

Carbon-supported copper GDEs could play a key role in the industrial development of ERCO₂ due to multiple factors. Copper represents an environmentally safer choice with respect to nickel or lead-based catalyst [17] and is less expensive than silver, gold, palladium or rhodium. Copper appears to be also a valid choice as a catalyst in the ERCO₂ process due to its catalytic versatility. Since the beginning of the ERCO₂ scientific analysis, both CO and various hydrocarbons were detected as products obtained using a copper foil catalyst [18]. Different copper catalysts resulted to promote the formation of saturated and unsaturated hydrocarbons, alcohols, formic acid, carbon monoxide and other light carbon compounds [19–21]. Those selectivity modifications on copper-based catalysts were reported to be linked with the catalyst morphology [4,22].

Copper GDEs may be produced both by the immobilization of previously synthesized copper nanostructures onto the gas diffusion layer (GDL) [23] or by direct growth of the copper nanostructures onto the GDL [14].

Direct electrodeposition of target metals on GDL could be a versatile method to produce nanostructured catalytic electrodes with the desired morphology [24–26]. Additive-mediated electroplating of copper on GDLs was previously studied in the context of

ERCO₂ [27], revealing copper GDEs' ability to produce a wide range of carbon-based compounds, but no strict selectivity towards a specific bulk chemical was observed.

The target of this work is a preliminary analysis of copper-based gas diffusion electrodes obtained by additive-mediated electrodeposition techniques and their selectivity for the preparation of carbon monoxide as sole ERCO₂ product.

Correlations between deposition conditions and catalyst morphology were analyzed and discussed. Particular attention was given to the action mechanism of the additives and their role in determining the overall catalytic morphology.

Subsequently, the electrodes were tested as catalyst for the ERCO₂ process in a pH neutral, aqueous electrolyte and the selectivity towards the production of carbon monoxide was estimated. Correlations between electrode selectivity and deposition conditions of the electrodes were found and discussed.

2. Materials and Methods

2.1. Catalyst Synthesis

A single-compartment three-electrode cell was used for the synthesis of nanostructured catalysts by electrodeposition. Carbon paper supports (Sigracet GDL 39 BC) with a surface area of 1 cm² and 4 cm² were used as working electrodes, graphite foils (99.8% Alfa Aesar, Haverhill, MA, USA) were used as counter-electrode and Ag/AgCl electrode (Ag/AgCl, R1/AG-AGCL/4MMSKT, Amel Instruments, Milano, Italy) working with 3.0 M KCl (99% Fluka, Charlotte, NC, USA) was used as reference. All the potentials reported through the manuscript are referring to the Ag/AgCl electrode. The electrodeposition cell was magnetically stirred and maintained at 25 °C. A galvanostatic regime was chosen for the electrodepositions. Three levels of deposition current density were tested: −2, −4 or −6 mA cm^{−2}. The deposition current was applied by a potentiostat (Ivium nStat, Ivium technologies, Eindhoven, The Netherlands) and automatically stopped when a charge of 4 C cm^{−2} was reached.

The role of additives was investigated using aqueous electrodeposition baths with 0.1 M CuSO₄ · 5H₂O (VWR Chemicals, Radnor, PA, USA, 99%) and the chosen additive at a concentration of 0.01 M. The additives tested were dodecyltrimethylammonium bromide (DTAB, Acros Organics, Fair Lawn, NJ, USA, 99%), 3,5-diamino-1,2,4-triazole (DAT, Alfa Aesar, 98%), and polyethylene glycol (PEG, medium molecular weight 3350 Da, BioUltra grade, Sigma, St. Louis, MO, USA). The bath's pH was regulated at 2.0 by addition of concentrated sulfuric acid (96%, Carlo Erba Reagents, Cornaredo, Italy). The baths with additives will be indicated as the DTAB bath, DAT bath and PEG bath, respectively. In addition, an electrodeposition bath without any additive was employed (unadditivated bath). Electrodeposited samples were washed with distilled water, rinsed with ethanol (96%, Carlo Erba Reagents) and then dried at room temperature. The performances of the nanostructured synthesized electrodes were benchmarked against copper foil (99.98%, Sigma Aldrich) electrodes of 1 cm² and 4 cm².

The effect of electrodeposition conditions on the morphology of the synthesized electrodes was observed by scanning electron microscopy (SEM), energy-dispersive X-ray mapping (EDX) and X-ray diffraction analyses (XRD). SEM measurements and EDX mapping were performed using a Zeiss AURIGA field-emission scanning electron microscope (HR-FESEM) equipped with a Bruker EDX apparatus. XRD analyses were performed in reflexion mode on a Bragg-Brentano θ - θ diffractometer (Rigaku Ultima plus) equipped with a copper-based X-ray lamp operating at 40 kV, 24 mA.

X-ray photoelectron spectroscopy (XPS) analysis was performed on selected electrodes using an Omicron NanoTechnology MXPS system and Mg $k\alpha$ photons ($h\nu = 1253.6$ eV). Quantitative ratios are expressed as atomic ratio normalized to atomic cross-sections. No sample show charge build-up under X-rays. Cu 2p curve fitting was obtained by making use of a same set of parameters (relative position among peaks, full width at half maximum).

2.2. Catalyst Testing

Linear sweep voltammeteries (LSV) were performed in a gas-tight H-cell divided in two compartments by a Nafion membrane (N-117, Alfa Aesar) was used. The same three-electrodes configuration described previously was adopted. The cathodic compartment of the cell was equipped with a gas bubbler and a manual vent valve. Electrodeposited electrodes of 1 cm² were tested in an aqueous electrolyte of 0.5 M KHCO₃ (99%, Alfa Aesar). Before each analysis, the electrolyte was bubbled with CO₂ (99.95%, SOL) for 20 min. LSV were carried out with the potential varying between −0.2 and −1.8 V at a scan rate of 50 mV s^{−1}.

The catalytic selectivity of the electrodes was estimated by analysing evolved gaseous products during chronoamperometric experiments. The electrochemical setup was the same employed in the LSV tests but, in addition, the cell was provided with a magnetic stirrer and a pierceable septum located on the lid. The electrolyte was used after 20 min of CO₂ saturation by bubbling. Before the beginning of the analysis the cell was sealed, and a potential of −1.4 V was applied to the tested electrode of 4 cm². The experiments were interrupted when a charge of 20 C was reached. The pressure of the cell was measured by a digital differential pressure meter (Digitron 2022 P). Gaseous reduction products were analyzed using a gas chromatograph (GC; Clarus 590, Perkin Elmer) equipped with a TCD detector. A series of two 2-meter columns, Hayesep Q and Shincarbon ST Micropacked (Restek), were used. Analytical grade argon (Rivoira, 99.9995%) was used as carrier. Gas sampling and evaluation was performed immediately after the end of the chronoamperometric session. Reduction selectivity towards carbon monoxide was estimated as faradaic efficiency.

3. Results and Discussion

3.1. Effect of the Additives on Catalysts Morphology

The effect of the additives on the electrodeposition process can be clarified by the analysis of the chronopotentiometric current data, i.e., the deposition potential trend measured during the electrodeposition processes. Chronopotentiometric profiles obtained under the effect of different additives are compared in Figure 1. The potential profile of a deposition obtained from an unadditivated bath is reported as reference.

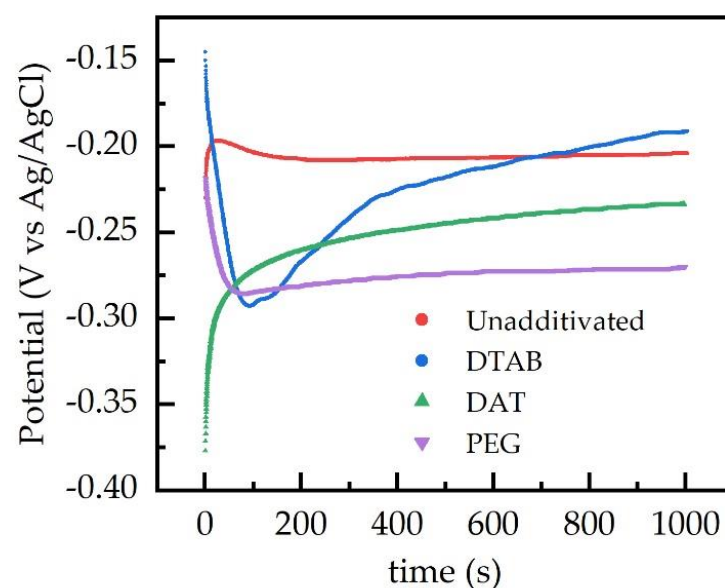


Figure 1. Chronopotentiometric curves of the deposition process, showing the variation of the electrode potential during the electrodeposition process. The deposition current density was -2 mA cm^{-2} .

The potential profile recorded during the electrodeposition from the copper bath without additives highlights an initial short phase of higher overpotential, due to the nucleation of copper particles on the carbon paper surface, and a following phase at constant potential, due to the growth of copper particles after their nucleation.

The potential profile obtained during the electrodeposition with DTAB baths shows three different sections: a short zone of high potential, a wide potential peak and a gradual potential decreasing. The high potential zone may be explained by the surfactant behavior of the additive. In fact, DTAB is a long-chain quaternary ammonium salt used as a cationic surfactant. The carbon paper structure is partially hydrophobic and thus, by adding a surfactant, a wider section of the carbon paper surface is accessible for the nucleation. The following peak underlines a strong inhibition at the beginning of the copper growth, caused by the adsorption of dodecyltrimethylammonium ions (DTA⁺) on the surface of the deposited metal, leading to the formation of micelle-like structures or hydrophobic double layers on the surface of the electrode [28]. This adsorption is partially due to the coulombic attraction between the additive ion and the electrode and is focused onto high current density areas on the electrode surface, such as crests and peaks. Adsorbed supramolecular structures hinder the copper deposition, thus limiting the formation of large three-dimensional structures on to the deposited metal [29].

Deposition potential slowly increases in the final part of the deposition; this may be explained by an increase in the electroactive surface area of the electrode.

The chronopotentiometric curve obtained from DAT baths reveals a low potential at the beginning of the Cu electrodeposition. This could be associated with an inhibition during the Cu nucleation phase. DAT is an aromatic triazole, known to form polycomplexes with copper ions in aqueous solutions [30] and to be easily adsorbed on the surface of metallic copper [31]. The inhibition is probably due to the formation of complexes and the consequent decrease of copper ions concentration available at the electrode surface.

Electrodeposition obtained from PEG baths were characterized by an initial phase of high potential and a following phase of low deposition potential. The high potential observed at the beginning of the deposition may be linked with its wetting properties: despite its structure not fulfilling the classical features of a surfactant, PEG addition is known to decrease the surface tension of aqueous solutions [32].

The subsequent zone of the chronopotentiometric curve represents the lowest Cu-deposition potential recorded among all the electrodeposition baths. This could be explained by the structure and the behaviour of PEG in aqueous solutions. PEG is a long-chain, water soluble polyether and its molecules may adsorb on to metallic copper, and copper ions in the deposition baths may be coordinated by oxygen atoms in the PEG structure. The electrodeposition of copper, on carbon paper areas covered by PEG, requires an intermediate step of ionic migration and partial reduction through the polymeric structure [33], inhibiting the deposition of metal.

Figure 2 offers a comparison between the different nanostructures obtained: geometrical aggregates from baths without additives (Figure 2a), nanospheres from the DTAB bath (Figure 2b), hemispheres of nanowires from the DAT bath (Figure 2c), and shapeless aggregates under the influence of the PEG bath (Figure 2d). Morphology of the Cu-depositions obtained from the unadditivated bath (containing only copper sulphate and sulfuric acid) were already observed on electrodepositions using similar baths on copper supports [34].

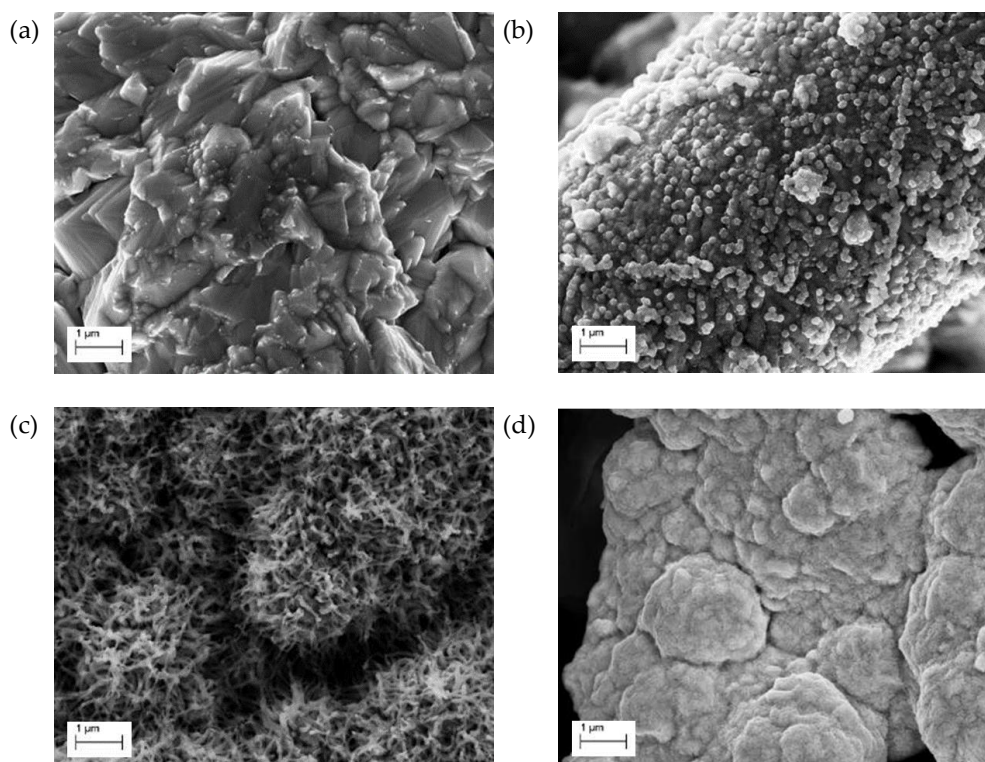


Figure 2. Scanning electron microscopy (SEM) images of the electrodeposited electrodes deposited at a current density of -2 mA cm^{-2} . Nanostructures obtained from: (a) unadditivated bath, (b) dodecyltrimethylammonium bromide (DTAB) bath, (c) 3,5-diamino-1,2,4-triazole (DAT) bath and (d) polyethylene glycol (PEG) bath.

These structures are commonly produced when the electrodeposition of copper films is under kinetic control [35], i.e., when the rate-limiting step of the electrodeposition is the reduction process on the surface of the electrode [36]. The electrodeposition carried out using the DTAB bath produce uniformly distributed nanospheres on the surface of the carbon fibers. Comparing these structures with those obtained from deposition without additives, it is possible to assert that DTAB baths enhance the copper nucleation processes, while the growth of the deposited structures is, at least partially, hindered. This is in agreement with the interpretation of chronopotentiometric analyses.

DAT morphological effects on copper electrodeposition are comparable with the observation of previous research [27]. The hemispherical distribution observed is probably due to a mixed control deposition regime [35]. The morphologic action of this additive is still unclear, but the chaotic wires pattern may be caused by a templating action induced by Cu-DAT polycomplexes. The formation of these porous, high-surface structures may be an explanation for the potential increase observed in the final part of the deposition curves (Figure 1). The structures obtained under the effect of PEG resulted in shapeless aggregates. PEG is commonly used as suppressing additive in the industrial electroplating process of copper [29]. Given the dimension of the polymeric chain, the adsorption of this molecule is limited to exposed areas of the deposition support, while its diffusion in the support pores is hindered. As previously stated, copper deposition is inhibited on the covered areas, while the deposition on pores is relatively unaffected due to the absence of adsorbed polymer. The global result is a levelling action on the deposition. The adsorption mechanism of PEG on to metallic copper is mainly evaluated in presence of chloride ions, but experiments suggest a wider range of possible co-ions [37].

3.2. Effect of the Electrodeposition Current Densities on Catalyst Morphology

In the case of DTAB-assisted depositions a decrease in the diameter of the nano spheres linked with the increasing of the current density was observed (Figure 3a,b). Higher current

densities are associated with more cathodic deposition potentials; these conditions promote nucleation processes, resulting in a finer grained deposition.

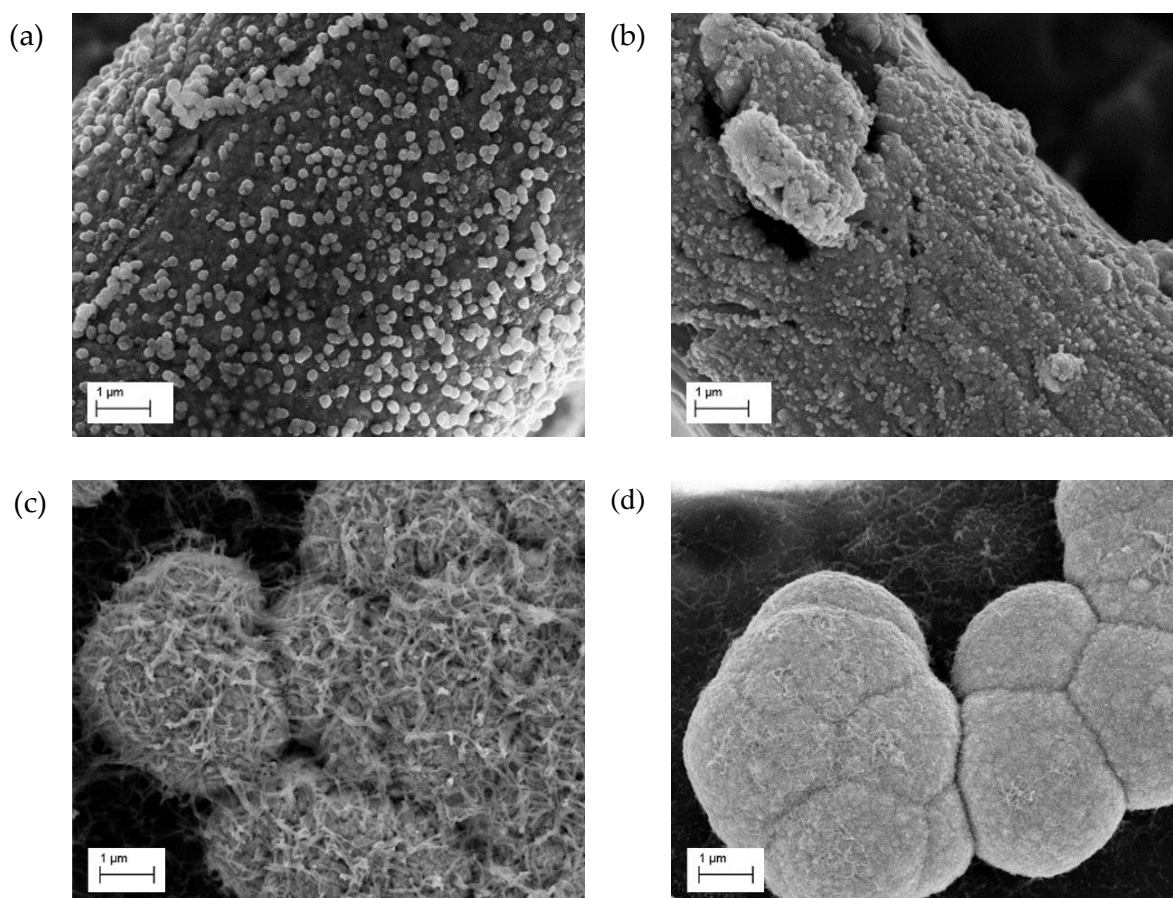


Figure 3. SEM images of the nanostructured electrodes obtained from DTAB (a,b) and DAT (c,d) baths. Deposition current density equal to -4 mA cm^{-2} (a,c) and -6 mA cm^{-2} (b,d).

On DAT-assisted depositions, an increase of the deposition current density causes a gradual disappearance of the nanowire structures and a transition towards hemispherical aggregates. This evolution is clearly visible in Figure 3c,d. Large hemispherical structures, obtained under the highest current density, are usually associated to mixed control systems, so the morphological modifications may be associated with a shifting of the deposition system towards a diffusive limitation [35]. Local modification of pH may also play a role, due to the pH influence on the stability of Cu-DAT complexes [27].

3.3. Energy-Dispersive X-ray Mapping (EDX), X-ray Diffraction Analyses (XRD) and X-ray Photoelectron Spectroscopy (XPS) Characterizations

In order to evaluate the copper distribution onto the carbon paper support and to underline the possible permanence of the deposition additives onto the catalyst structure, EDX mapping analyses were performed. EDX mapping and quantitative results for all the electrodes are reported in Figures S2–S6 of the Supporting Information File. Remarkably, in Figure 4, EDX mapping of electrodes coming from DAT and DTAB baths are reported. Nitrogen mapping of DAT electrode reveals a homogenous distribution of nitrogen on to the copper layer. Pristine carbon paper is completely nitrogen-free, thus the detected nitrogen indicates the presence of residual DAT. Its permanence outlines a partial inclusion of the additive into the copper catalyst during the deposition process. On the other hand, the presence of nitrogen species resulting after DAT decomposition/reaction during the electrodeposition cannot be excluded. In fact, electro-induced polymerization of DAT

and similar azoles was observed and studied on the surface of metal and carbon-based electrodes [38,39]. Likewise, the EDX mapping of DTAB electrode revealed the presence of bromine overlaid on the deposition of copper, indicating the inclusion of DTAB into the nanostructure.

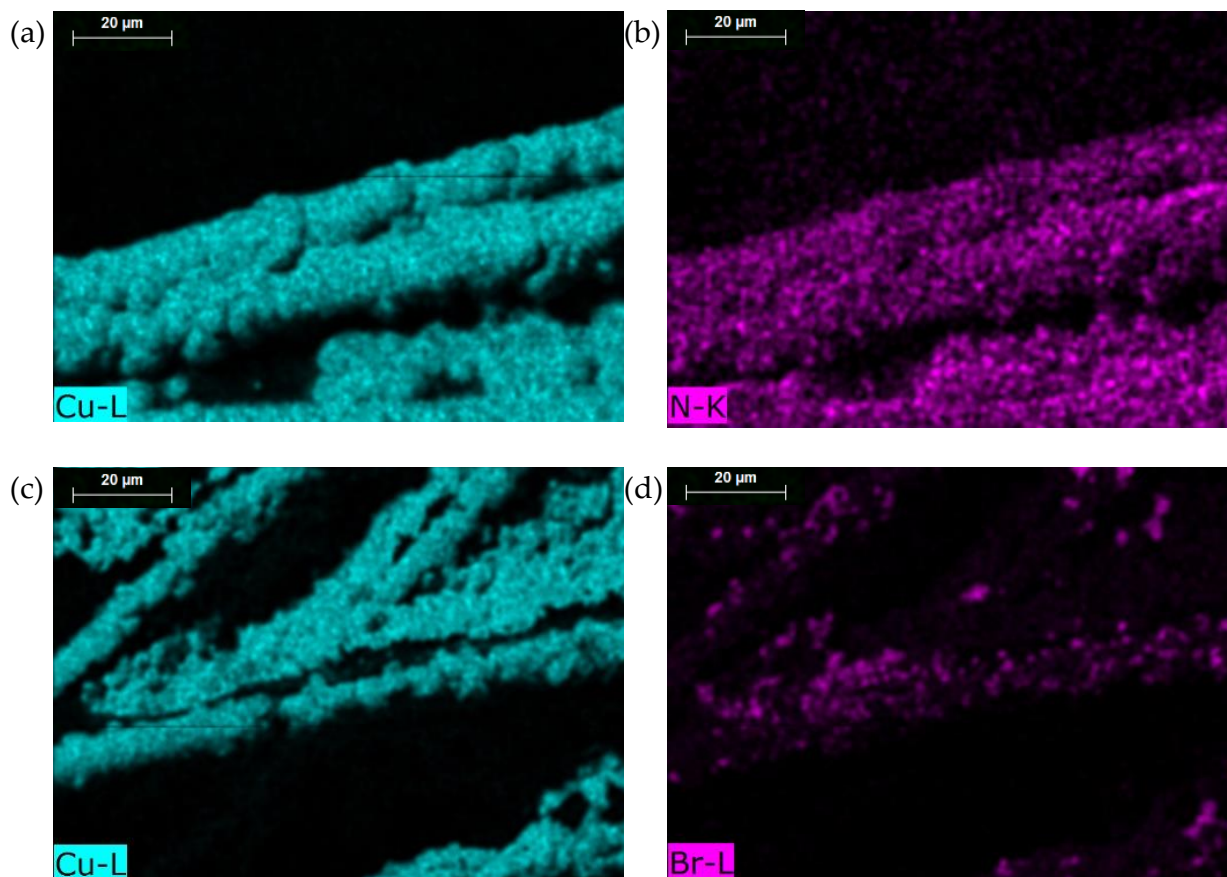


Figure 4. Energy-dispersive X-ray (EDX) surface mapping of an electroplated electrode obtained from DAT (a,b) and DTAB (c,d) baths.

XRD analyses were performed on the electrodes in order to obtain information on the crystallographic structure of the catalysts. A blank analysis was performed on to an undeposited carbon paper support, to discriminate between background diffraction peaks and deposition-related peaks. XRD analysis results are reported in Figure 5a. Peaks identified as copper-related are marked with an asterisk (*) and are associated with the presence of crystalline metallic copper [40]. While any electrode manifested the presence of metallic copper, no peaks associated with copper (I) or (II) compounds were observed. This result could be related to the low amount of oxidized Cu species and/or their amorphous nature. A partial oxidation of the electrode surface is expected due to metallic copper reaction with atmospheric oxygen and aqueous electrolyte, but this oxidation is expected to be limited to a thin layer in proximity of the deposit surface. Oxidized species are thus present as a small fraction of the total copper and, if present, would not be detectable by diffraction analyses. Nonetheless, XRD data underline a significant difference between the electrodeposited electrodes. A similar diffraction pattern is observed on electrodes produced from an unadditivated bath and electrodes obtained from DTAB baths with additives. The presence of sharp and well-defined copper-associated peaks suggests that the bulk structure of the deposited copper is composed of metallic crystalline copper. PEG-derived electrodes reveal a similar pattern, characterized by a lower peak intensity. Electrodes obtained from a DAT bath show the widest and lowest Cu peaks, revealing the presence of lower copper amount and probably its amorphous structures.

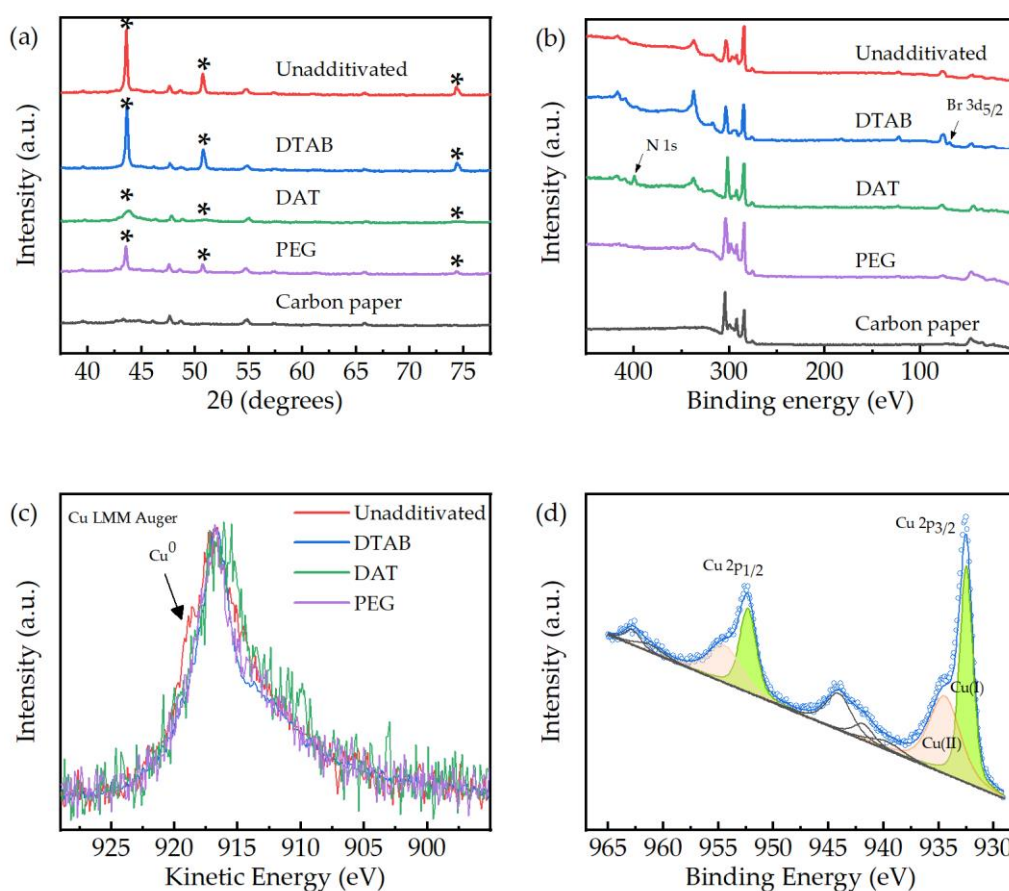


Figure 5. X-ray characterization of the electroplated electrodes. The electrodes were deposited under a current density of 2 mA cm^{-2} . (a) X-ray diffraction (XRD) analyses of electrodeposited electrodes compared with a carbon paper foil. The * mark identifies copper diffraction peaks. (b) Wide-angle X-ray photoelectron spectroscopy (XPS) analyses of the electrodes. (c) X-ray excited Cu LMM Auger peaks for the various electrodes. (d) Deconvolution of the XPS data, DTAB-assisted electrode.

It is well known that when no faradaic contribution from the catalyst is involved, the only electroactive species during ER CO_2 are those present onto the surface of the deposited nanostructure. To clarify the surface chemical state of Cu and to afford the relative quantitative ratios among all the constituent elements, XPS measurements have been applied to the full series of electrodes (Figure 5b). Table S4 of supplementary information file shows the further relevant data. Copper was present as both Cu(I) and Cu(II) species, as inferred by curve fitting the complex Cu 2p envelope (Figure 5d). A notable exception is the case of the electrodes synthesized without additives, for which the presence of Cu(0) was additionally inferred by the evident shoulder in the CuLMM Auger peak (Figure 5c), since Cu(0) and Cu(I) present the same binding energy and line shape. Copper was quantified by calculating ratios of the areas of Cu 2p $_{3/2}$ against the sole C 1s components related to the carbon paper substrate. The largest and smallest Cu/C relative amounts were respectively found for DTAB and PEG electrodes, while comparable amounts were obtained for electrodes obtained from unadditivated and DAT baths. The Cu(I)/Cu(II) ratios was highest for DTAB, comparable for PEG and unadditivated baths, and smallest for DAT. Evidence for the presence of bromides was reached only for DAT, as expected, while sulphates and organic nitrogen were present in the case of DTAB (Figure 5b).

3.4. Catalysts Evaluation

In an aqueous electrolyte ER CO_2 may be affected by side reactions and a competition between reduction of carbon dioxide to carbon monoxide ($-0.74 \text{ V}_{\text{pH}7}$ vs. Ag/AgCl) and reduction of water to hydrogen ($-0.63 \text{ V}_{\text{pH}7}$) is expected. Besides the electrolyte decom-

position, the ER CO_2 process could also lead to the formation of other carbon compounds, such as methane ($-0.45 V_{\text{pH}7}$), formic acid ($-0.82 V_{\text{pH}7}$) and methanol ($-0.59 V_{\text{pH}7}$) [7]. A suitable catalyst should have the highest selectivity towards the production of CO, that implies low overpotentials for the reaction of interest with respect to the equilibrium Nernst potential. The properties of the electrodeposited electrodes may be preliminarily observed by LSV analysis, indicating the occurrence of reduction peaks/currents and onset reduction potentials. LSV analyses of electrodeposited electrodes, compared with a flat copper foil electrode, are reported in Figure 6. It is important to underline that the electrodes tested on LSV were not operating as GDE, but as solid–liquid electrodes, receiving the carbon dioxide required from the saturated electrolytic solution.

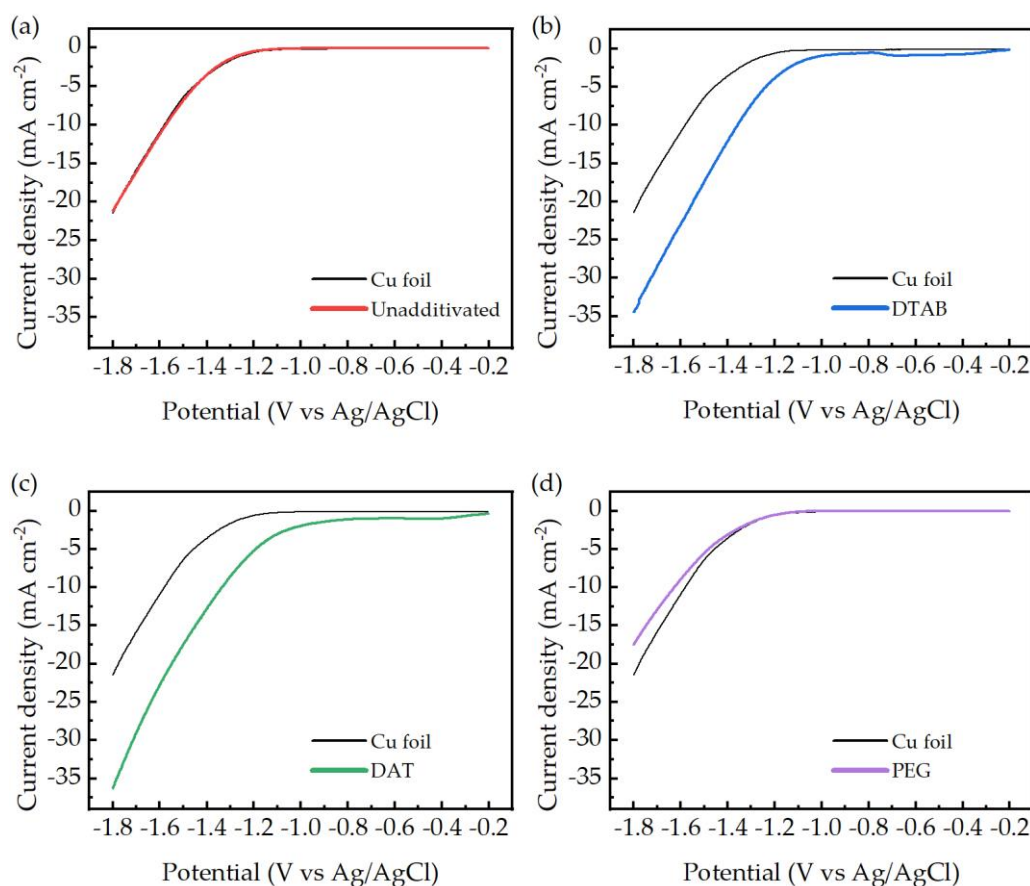


Figure 6. Linear sweep voltammeteries (LSV) analysis of the electrodeposited electrodes obtained from unadditivated bath (a), DTAB (b), DAT (c) and PEG (d) compared to copper foil LSV (red lines).

The potential range of interest starts in the close proximity of the standard potential of the carbon dioxide reduction to carbon monoxide ($-0.74 V_{\text{pH}7}$). This value represents the thermodynamic limit of the reduction reaction. The actual reaction is expected to be observed at more cathodic potentials.

Copper foil electrodes do not show visible reduction peaks, and their onset potential is approximately 1.2 V. Electrodes obtained from DTAB and DAT baths display both the presence of reduction peaks (only partially visible for the DAT electrode) and lower onset reduction potentials compared to the copper foil, of approximately $-0.3 V$. Even if a clear assignation of the reductive peaks was not possible due to strict similarities in the standard potential of the possible reactions, their presence is a clear sign of a diffusion-limited reduction process, compatible with the adsorption and the electroreduction of CO_2 to CO onto the catalytic electrodes. Low onset potentials are associated with a decrease in the activation energy required from the reduction process; this suggests the formation of low-energy intermediates on the catalyst surface.

LSVs of electrodes obtained from a bath without additives and a PEG bath were almost identical to copper foil curves, thus indicating a lack of specific catalytic activity. During ER CO_2 tests the formation of various gaseous products is possible, so GC analysis is required to determine which products were obtained under the tested conditions. GC analysis confirmed the presence of only hydrogen and carbon monoxide as detectable gaseous product and the absence of higher carbon compounds.

Selectivity tests were performed in two subsequent steps: batch chronoamperometry and GC analysis. The results were reported for any electrodes' deposition conditions and compared in Figure 7a.

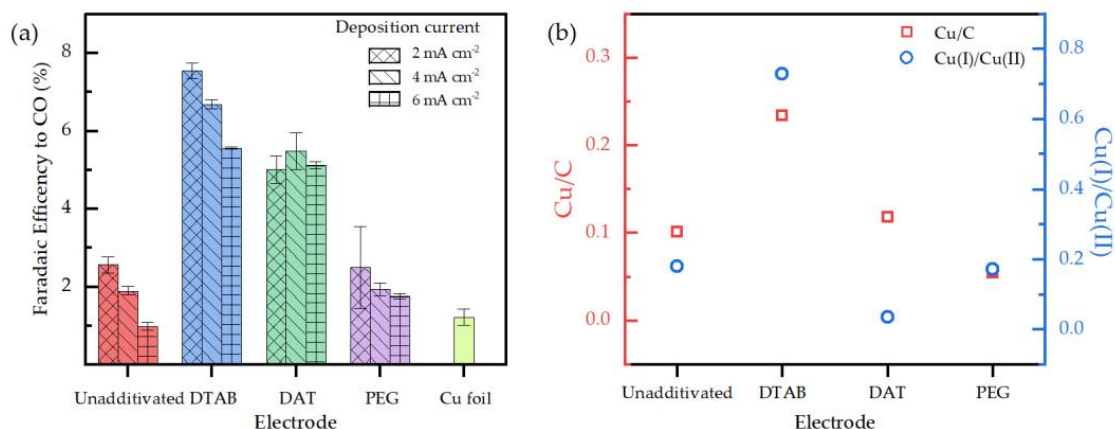


Figure 7. (a) Catalysts selectivity towards the production of CO of the nanostructured electrodes reported as faradaic efficiency. Selectivity of the copper foil electrode is reported as a comparison. (b) Cu/C and Cu(I)/Cu(II) ratio derived from XPS analysis. In the case of unadditivated electrode Cu(0) amount was added to Cu(I).

Electrodes synthesized without additives expressed selectivity levels close to the copper foil electrode. These results underline a scarce difference between copper foil and unadditivated electroplated copper catalytic properties. The exposed crystalline planes of those structures may be comparable, both qualitatively and quantitatively, and the catalysts specific surface could be similar.

Electrodes obtained from DTAB and DAT baths show the higher selectivity values. The nanospheres obtained by DTAB-mediated electrodeposition showed a six-fold increase in faradaic efficiency towards the carbon monoxide compared to the copper foil, while DAT-derived nanowires aggregates expressed a four-fold increase. Electrodes synthesized from PEG baths do not differ strictly from unadditivated electrodes. These results are in agreement with LSV analyses.

Considering the Cu/C ratio (Figure 7b) as the amount of Cu on the electrodes surface, DAT electrodes displays an unexpected high selectivity among the electrodes. A Cu/C ratio about two times lower than DTAB was found for the DAT electrode, while the selectivity is lower by just 27%. This result may be explained by considering both its peculiar morphology and its crystalline structure. In fact, the nanowires array presents a high surface-to-volume ratio (Figure 2c) and could be linked with an increase in the active surface if compared to an equal mass of other copper-based catalysts. In addition, XRD analysis of DAT electrodes revealed the presence of amorphous copper distinctly different from the other electroplated electrodes (Figure 5a).

Additionally, the catalytic activity of DAT-derived electrodes may be also linked with the partial incorporation of DAT molecules into the deposit structure, as observed both from EDX and XPS analyses (Figures 4 and 5b). Catalytic activity towards ER CO_2 was previously observed onazole-metal complexes [41] so the simultaneous catalytic action of metallic copper and DAT-copper compounds cannot be excluded. Catalytic properties of DAT-mediated electrodeposited electrodes were already observed in literature [27] but those structures were only deposited on to flat supports such as metallic foils or carbon

nanoparticles sheets. To the best of our knowledge, DAT-assisted electroplated structures had never been electrodeposited on to an inhomogeneous support such as carbon paper fibers. Remarkably, in contrast with the literature data, a higher selectivity towards the production of CO was observed for electrodes obtained from DTAB-assisted depositions.

The highest selectivity related to DTAB electrodes could be explained taking into account several parameters. (1) Surfactant action of DTAB could have increased the carbon paper surface area available for the electrodeposition for a given electrode dimension. This led to the highest Cu/C ratio for the DTAB electrode (Figure 7b). (2) The nanospheres pattern (Figure 3a) itself is porous and increases the specific surface of the catalyst. (3) A contribution to the catalytic properties may also come from the additive incorporated onto the copper structure. Similar to DAT, catalytic properties of adsorbed DTAB were previously observed on metallic catalysts in the ERCO₂ process. The DTAB presence was associated with an increase in the production of CO, probably due to the inhibition of hydrogen evolution [42].

Low selectivity observed on a catalyst obtained from PEG bats could be explained by PEG inhibitive behavior during the electrodeposition process that results in the lowest Cu amount on the electrodes surface as displayed from the Cu/C ratio in Figure 7b.

No direct correlation between the Cu(I)/Cu(II) ratio (Figure 7b) and selectivity can be attributed. DTAB and DAT electrodes showed the highest selectivity among the electrodes and were characterized by the highest and lowest Cu(I)/Cu(II) ratio, respectively.

This was probably due to the reduction of Cu(I) and Cu(II) compounds into metallic copper during the electroreduction process, as previously observed on an oxide-based catalyst [43].

No significant variation in selectivity was observed with DAT electrodes produced at different current densities. According to this result, nanowires length does not seem to influence the selectivity of the catalytic structures. On the other hand, a strong correlation between deposition current density and selectivity was observed for the electrodes synthesized from DTAB baths. As Figure 7a shows, a decrease in the deposition current from 6 mA cm⁻² to 2 mA cm⁻² is associated with a 25% increase in the catalyst selectivity. An increase of the deposition current density is commonly associated with an overpotential rise and a consequential decrease in the amount of deposited metal is expected.

Regarding the electrode morphology, a reduction in the size of copper nanoparticles has been associated with an increase in the catalyst selectivity. This phenomenon could be due to a modification of the exposed crystallographic planes on the surface of the catalyst and has been documented as a cause of selectivity modifications [44]. This is in accordance with our observations (Figures 3a,b and 7a).

4. Conclusions

Nanostructured electrocatalysts for the ERCO₂ process were synthesized by electrodeposition of copper onto a carbon paper support. The effect of different deposition conditions and deposition additives was analyzed.

Deposition using additives proved to be an effective nanostructuring synthesis method. Hemispherical aggregates of nanowires were synthesized employing DAT, while nanospheres were obtained by DTAB-mediated deposition and shapeless structures were obtained from PEG-mediated depositions. A correlation between deposition current density and catalysts morphology was observed.

Catalytic selectivity tests of the electrodeposited electrodes underlined a general increase in the selectivity towards the production of carbon monoxide compared to a copper foil electrode. Deposition additives resulted in playing a critical role in the selectivity of the electrodes. Catalysts obtained from DAT baths showed a four-fold increase of the selectivity, while catalysts produced from DTAB baths reached a six-fold increase.

No significant effect of Cu(I)/Cu(II) ratio was found on the selectivity of the electrodes, while the effect of electrodeposition current density was related to the specific additive.

In conclusion, electrodes obtained from DTAB baths under a deposition current density of 2 mA cm^{-2} proved to be the most selective towards the production of carbon dioxide.

Supplementary Materials: The following are available online at <https://www.mdpi.com/article/10.3390/en14165012/s1>, Figure S1: SEM images of carbon paper fibers. Magnification factor of (a) 150:1 and (b) 500:1, Figure S2: EDX surface mapping of the carbon paper support. (a) SEM image of carbon paper fibers; (b) Carbon mapping; (c) Fluorine mapping; (d) Oxygen mapping, Figure S3: EDX surface mapping of an electroplated electrode obtained from unadditivated baths. Deposition current density 2 mA cm^{-2} . (a) SEM image of the electrode; (b) Carbon mapping; (c) Fluorine mapping; (d) Oxygen mapping; (e) Copper mapping, Figure S4: EDX surface mapping of an electroplated electrode obtained from DTAB-additivated baths. Deposition current density 2 mA cm^{-2} . (a) SEM image of the electrode; (b) Carbon mapping; (c) Fluorine mapping; (d) Oxygen mapping; (e) Copper mapping; (f) Bromine mapping, Table S1: EDX elemental analysis of an electroplated electrode obtained from DTAB-additivated baths. Deposition current density 2 mA cm^{-2} , Table S2: EDX elemental analysis of an electroplated electrode obtained from DAT-additivated baths. Deposition current density 2 mA cm^{-2} , Figure S6: EDX surface mapping of an electroplated electrode obtained from PEG-additivated baths. Deposition current density 2 mA cm^{-2} . (a) SEM image of the electrode; (b) Carbon mapping; (c) Fluorine mapping; (d) Oxygen mapping; (e) Copper mapping; (f) Nitrogen mapping, Table S3: EDX elemental analysis of an electroplated electrode obtained from PEG-additivated baths. Deposition current density 2 mA cm^{-2} , Table S4: Atomic ratios between the main components found with XPS quantitative analysis. Cu(I)/Cu(II) ratio for NOADD electrode refers to $[\text{Cu}(0)+\text{Cu}(I)]/\text{Cu}(II)$, Figure S7: XPS Cu 2p spectra from the unadditivated electrode. Current density of deposition: -2 mA cm^{-2} , Figure S8: Cu 2p XPS spectra from the DAT electrode. Current density of deposition: -2 mA cm^{-2} , Figure S9: Cu 2p XPS spectra from the PEG electrode. Current density of deposition: -2 mA cm^{-2} .

Author Contributions: Conceptualization, G.Z. and P.G.S.; methodology, G.Z., R.Z. and A.R.; validation, F.P. and P.A.; investigation, G.Z.; resources, F.P.; data curation, G.Z. and P.G.S.; writing—original draft preparation, G.Z. and P.G.S.; writing—review and editing, G.Z. and P.G.S.; visualization, P.A. and F.P.; supervision, F.P. All authors have read and agreed to the published version of the manuscript.

Funding: This research received no external funding.

Data Availability Statement: Data is contained within the article.

Conflicts of Interest: The authors declare no conflict of interest.

References

1. British Petroleum Co. *BP Statistical Review of World Energy*; British Petroleum Co.: London, UK, 2019.
2. Liu, Y.; Huo, Z.; Sun, D.; Chen, R.; Chen, Y.; Basu, S.; Hong, F.; Jin, F.; Wang, X.; Qiao, J.; et al. *Electrochemical Reduction of Carbon Dioxide: Fundamentals and Technologies*; CRC Press: Boca Raton, FL, USA, 2016; ISBN 9781482258240.
3. Hori, Y.; Wakebe, H.; Tsukamoto, T.; Koga, O. CO_2 Reduction on Metals. *Electrochim. Acta* **1994**, *39*, 1833–1839. [[CrossRef](#)]
4. Tang, W.; Peterson, A.A.; Varela, A.S.; Jovanov, Z.P.; Bech, L.; Durand, W.J.; Dahl, S.; Nørskov, J.K.; Chorkendorff, I. The importance of surface morphology in controlling the selectivity of polycrystalline copper for CO_2 electroreduction. *Phys. Chem. Chem. Phys.* **2012**, *14*, 76–81. [[CrossRef](#)]
5. Tan, X.; Yu, C.; Ren, Y.; Cui, S.; Li, W.; Qiu, J. Recent advances in innovative strategies for the CO_2 electroreduction reaction. *Energy Environ. Sci.* **2021**, *14*, 765–780. [[CrossRef](#)]
6. Zheng, T.; Jiang, K.; Ta, N.; Hu, Y.; Zeng, J.; Liu, J.; Wang, H. Large-Scale and Highly Selective CO_2 Electrocatalytic Reduction on Nickel Single-Atom Catalyst. *Joule* **2019**, *3*, 265–278. [[CrossRef](#)]
7. Lu, Q.; Jiao, F. Electrochemical CO_2 reduction: Electrocatalyst, reaction mechanism, and process engineering. *Nano Energy* **2016**. [[CrossRef](#)]
8. Malik, K.; Singh, S.; Basu, S.; Verma, A. Electrochemical reduction of CO_2 for synthesis of green fuel. *Wiley Interdiscip. Rev. Energy Environ.* **2017**, *6*, e244. [[CrossRef](#)]
9. Wang, Y.; Zhou, J.; Lv, W.; Fang, H.; Wang, W. Electrochemical reduction of CO_2 to formate catalyzed by electroplated tin coating on copper foam. *Appl. Surf. Sci.* **2016**, *362*, 394–398. [[CrossRef](#)]
10. Lamaison, S.; Wakerley, D.; Blanchard, J.; Montero, D.; Rousse, G.; Mercier, D.; Marcus, P.; Taverna, D.; Giaume, D.; Mougel, V.; et al. High-Current-Density CO_2 -to- CO Electroreduction on Ag-Alloyed Zn Dendrites at Elevated Pressure. *Joule* **2020**, *4*, 395–406. [[CrossRef](#)]
11. Morimoto, M.; Takatsuji, Y.; Yamasaki, R.; Hashimoto, H.; Nakata, I.; Sakakura, T.; Haruyama, T. Electrodeposited Cu-Sn Alloy for Electrochemical CO_2 Reduction to CO/HCOO^- . *Electrocatalysis* **2018**, *9*, 323–332. [[CrossRef](#)]

12. Marepally, B.C.; Ampelli, C.; Genovese, C.; Tavella, F.; Quadrelli, E.A.; Perathoner, S.; Centi, G. Electrocatalytic reduction of CO₂ over dendritic-type Cu- And Fe-based electrodes prepared by electrodeposition. *J. CO₂ Util.* **2020**, *35*, 194–204. [[CrossRef](#)]
13. O'Hayre, R.; Cha, S.-W.; Colella, W.; Prinz, F.B. *Fuel Cell Fundamentals*, 3rd ed.; John Wiley & Sons: Hoboken, NJ, USA, 2016.
14. Dinh, C.T.; Burdyny, T.; Kibria, G.; Seifitokaldani, A.; Gabardo, C.M.; Pelayo García De Arquer, F.; Kiani, A.; Edwards, J.P.; De Luna, P.; Bushuyev, O.S.; et al. CO₂ electroreduction to ethylene via hydroxide-mediated copper catalysis at an abrupt interface. *Science* **2018**, *360*, 783–787. [[CrossRef](#)]
15. Möller, T.; Ju, W.; Bagger, A.; Wang, X.; Luo, F.; Ngo Thanh, T.; Varela, A.S.; Rossmeisl, J.; Strasser, P. Efficient CO₂ to CO electrolysis on solid Ni-N-C catalysts at industrial current densities. *Energy Environ. Sci.* **2019**, *12*, 640–647. [[CrossRef](#)]
16. Ma, M.; Clark, E.L.; Therkildsen, K.T.; Dalsgaard, S.; Chorkendorff, I.; Seger, B. Insights into the carbon balance for CO₂ electroreduction on Cu using gas diffusion electrode reactor designs. *Energy Environ. Sci.* **2020**, *13*, 977–985. [[CrossRef](#)]
17. Farago, M.E. (Ed.) *Plants and the Chemical Elements: Biochemistry, Uptake, Tolerance and Toxicity*; VCH Publishers: New York, NY, USA, 1995; Volume 87, ISBN 3527282696.
18. Hori, Y.; Murata, A.; Takahashi, R. Formation of hydrocarbons in the electrochemical reduction of carbon dioxide at a copper electrode in aqueous solution. *J. Chem. Soc. Faraday Trans. 1 Phys. Chem. Condens. Phases* **1989**, *85*, 2309–2326. [[CrossRef](#)]
19. Jiao, J.; Lin, R.; Liu, S.; Cheong, W.C.; Zhang, C.; Chen, Z.; Pan, Y.; Tang, J.; Wu, K.; Hung, S.F.; et al. Copper atom-pair catalyst anchored on alloy nanowires for selective and efficient electrochemical reduction of CO₂. *Nat. Chem.* **2019**, *11*, 222–228. [[CrossRef](#)]
20. Taehee, K.; Palmore, G.T.R. A scalable method for preparing Cu electrocatalysts that convert CO₂ into C₂+ products. *Nat. Commun.* **2020**, *11*. [[CrossRef](#)]
21. Kwon, Y.; Lum, Y.; Clark, E.L.; Ager, J.W.; Bell, A.T. CO₂ Electroreduction with Enhanced Ethylene and Ethanol Selectivity by Nanostructuring Polycrystalline Copper. *ChemElectroChem* **2016**, *3*, 1012–1019. [[CrossRef](#)]
22. Yang, K.D.; Ko, W.R.; Lee, J.H.; Kim, S.J.; Lee, H.; Lee, M.H.; Nam, K.T. Morphology-Directed Selective Production of Ethylene or Ethane from CO₂ on a Cu Mesopore Electrode. *Angew. Chem.-Int. Ed.* **2017**, *129*, 814–818. [[CrossRef](#)]
23. Zhang, J.; Luo, W.; Züttel, A. Self-supported copper-based gas diffusion electrodes for CO₂ electrochemical reduction. *J. Mater. Chem. A* **2019**, *7*, 26285–26292. [[CrossRef](#)]
24. Pagnanelli, F. Shape evolution and effect of organic additives in the electrosynthesis of Cu nanostructures. *J. Solid State Electrochem.* **2019**, *23*, 2723–2735. [[CrossRef](#)]
25. Schiavi, P.G.; Rubino, A.; Altimari, P.; Pagnanelli, F. Two electrodeposition strategies for the morphology-controlled synthesis of cobalt nanostructures. *AIP Conf. Proc.* **2018**, 020005. [[CrossRef](#)]
26. Schiavi, P.G.; Farina, L.; Altimari, P.; Navarra, M.A.; Zanoni, R.; Panero, S.; Pagnanelli, F. A versatile electrochemical method to synthesize Co-CoO core-shell nanowires anodes for lithium ion batteries with superior stability and rate capability. *Electrochim. Acta* **2018**, *290*, 347–355. [[CrossRef](#)]
27. Hoang, T.T.H.; Ma, S.; Gold, J.I.; Kenis, P.J.A.; Gewirth, A.A. Nanoporous Copper Films by Additive-Controlled Electrodeposition: CO₂ Reduction Catalysis. *ACS Catal.* **2017**, *7*, 3313–3321. [[CrossRef](#)]
28. Jo, Y.E.; Yu, D.Y.; Cho, S.K. Revealing the inhibition effect of quaternary ammonium cations on Cu electrodeposition. *J. Appl. Electrochem.* **2020**, *50*, 245–253. [[CrossRef](#)]
29. Kondo, K.; Akolkar, R.N.; Barkey, D.P.; Masayuki, Y. *Copper Electrodeposition for Nanofabrication of Electronics Devices*; Springer: Berlin/Heidelberg, Germany, 2014; ISBN 978-1-4614-9176-7.
30. Aznar, E.; Ferrer, S.; Borrás, J.; Lloret, F.; Liu-González, M.; Rodríguez-Prieto, H.; García-Granda, S. Coordinative versatility of guanazole [3,5-diamino-1,2,4-triazole]: Synthesis, crystal structure, EPR, and magnetic properties of a dinuclear and a linear trinuclear copper(II) complex containing small bridges and triazole ligands. *Eur. J. Inorg. Chem.* **2006**, 5115–5125. [[CrossRef](#)]
31. Guo, L.; Dong, W.; Zhang, S. Theoretical challenges in understanding the inhibition mechanism of copper corrosion in acid media in the presence of three triazole derivatives. *RSC Adv.* **2014**, *4*, 41956–41967. [[CrossRef](#)]
32. Sobisch, T. The use of methyl orange for the characterization of micelles in aqueous nonionic surfactant solutions. In *Trends in Colloid and Interface Science VI*; Helm, C., Lösche, M., Möhwald, H., Eds.; Progress in Colloid & Polymer Science, Steinkopff; The Electrochemical Society: Pennington, NJ, USA, 2007; Volume 89.
33. Hebert, K.R.; Adhikari, S.; Houser, J.E. Chemical Mechanism of Suppression of Copper Electrodeposition by Poly(ethylene glycol). *J. Electrochem. Soc.* **2005**, *152*, C324. [[CrossRef](#)]
34. Isa, N.N.C.; Mohd, Y.; Zaki, M.H.M.; Mohamad, S.A.S. Characterization of copper coating electrodeposited on stainless steel substrate. *Int. J. Electrochem. Sci.* **2017**. [[CrossRef](#)]
35. Guo, L.; Oskam, G.; Radisic, A.; Hoffmann, P.M.; Searson, P.C. Island growth in electrodeposition. *J. Phys. D Appl. Phys.* **2011**, *44*. [[CrossRef](#)]
36. Altimari, P.; Schiavi, P.G.; Rubino, A.; Pagnanelli, F. Electrodeposition of cobalt nanoparticles: An analysis of the mechanisms behind the deviation from three-dimensional diffusion-control. *J. Electroanal. Chem.* **2019**, 851. [[CrossRef](#)]
37. Rooney, R.T.; Jha, H.; Rohde, D.; Schmidt, R.; Gewirth, A.A. Suppression of Copper Electrodeposition by PEG in Methanesulfonic Acid Electrolytes. *J. Electrochem. Soc.* **2019**, *166*, D551–D558. [[CrossRef](#)]
38. Kesavan, S.; Abraham John, S. Fabrication of aminotriazole grafted gold nanoparticles films on glassy carbon electrode and its application towards the simultaneous determination of theophylline and uric acid. *Sens. Actuators B Chem.* **2014**, *205*, 352–362. [[CrossRef](#)]

39. Calam, T.T. Electrochemical Oxidative Determination and Electrochemical Behavior of 4-Nitrophenol Based on an Au Electrode Modified with Electro-polymerized 3,5-Diamino-1,2,4-triazole Film. *Electroanalysis* **2020**, *32*, 149–158. [[CrossRef](#)]
40. Zhang, K.; Alexandrov, I.V.; Valiev, R.Z.; Lu, K. Structural characterization of nanocrystalline copper by means of x-ray diffraction. *J. Appl. Phys.* **1996**, *80*, 5617–5624. [[CrossRef](#)]
41. Williams, C.K.; Lashgari, A.; Chai, J.; Jiang, J. “Jimmy” Enhanced Molecular CO₂ Electroreduction Enabled by a Flexible Hydrophilic Channel for Relay Proton Shuttling. *ChemSusChem* **2020**, *13*, 3412–3417. [[CrossRef](#)]
42. Quan, F.; Xiong, M.; Jia, F.; Zhang, L.; Quan, F.; Xiong, M.; Jia, F.; Zhang, L. Efficient electroreduction of CO on bulk silver electrode in aqueous solution via the inhibition of hydrogen evolution. *Appl. Surf. Sci.* **2017**, *399*, 48–54. [[CrossRef](#)]
43. Handoko, A.D.; Ong, C.W.; Huang, Y.; Lee, Z.G.; Lin, L.; Panetti, G.B.; Yeo, B.S. Mechanistic insights into the selective electroreduction of carbon dioxide to ethylene on Cu₂O-derived copper catalysts. *J. Phys. Chem. C* **2016**, *120*, 20058–20067. [[CrossRef](#)]
44. Reske, R.; Mistry, H.; Behafarid, F.; Roldan Cuenya, B.; Strasser, P. Particle size effects in the catalytic electroreduction of CO₂ on Cu nanoparticles. *J. Am. Chem. Soc.* **2014**, *136*, 6978–6986. [[CrossRef](#)] [[PubMed](#)]